THE JOURNAL OF PHYSICAL CHEMISTRY LETTERS
A JOURNAL OF THE AMERICAN CHEMICAL SOCIETY

pubs.acs.org/JPCL
Letter

Deciphering Density Fluctuations in the Hydration Water of Brownian Nanoparticles via Upconversion Thermometry

Fernando E. Maturi, Ramon S. Raposo Filho, Carlos D. S. Brites, Jingyue Fan, Ruihua He, Bilin Zhuang, Xiaogang Liu,* and Luís D. Carlos*

Cite This: J. Phys. Chem. Lett. 2024, 15, 2606−2615
Read Online

ABSTRACT: We investigate the intricate relationship among temperature, pH, and Brownian velocity in a range of differently sized upconversion nanoparticles (UCNPs) dispersed in water. These UCNPs, acting as nanorulers, offer insights into assessing the relative proportion of high-density and low-density liquid in the surrounding hydration water. The study reveals a size-dependent reduction in the onset temperature of liquid-water fluctuations, indicating an augmented presence of high-density liquid domains at the nanoparticle surfaces. The observed upper-temperature threshold is consistent with a hypothetical phase diagram of water, validating the two-state model. Moreover, an increase in pH disrupts the organization of water molecules, similar to external pressure effects, allowing simulation of the effects of temperature and pressure on hydrogen bonding networks. The findings underscore the significance of the surface of suspended nanoparticles for understanding high- to low-density liquid fluctuations and water behavior at charged interfaces.

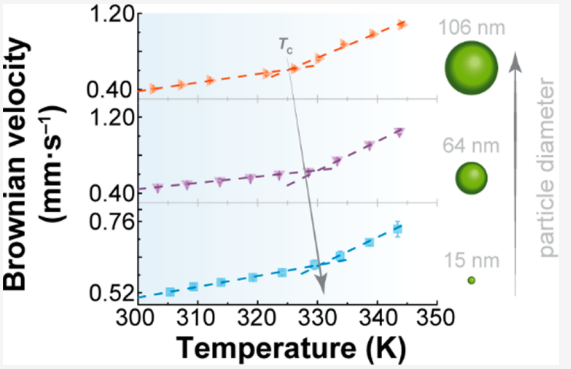

Liquid water is the main constituent of the human body and covers a majority of the Earth's surface. It plays a vital role in a myriad of biological, chemical, physical, geological, industrial, and environmental processes.[1−7] In addition to its chemical properties as a solvent, proton transfer medium, and active component of reactions, the physical properties of water are also fundamentally relevant.[8] Although water is the most commonly used liquid, its complex behavior under varying pressure and temperature conditions leads to numerous anomalies in its properties that differ significantly from those of other commonly used liquids. To date, more than 60 anomalous properties have been reported for water,[9−12] including a minimum specific heat at 308 K, a negative thermal expansion coefficient below 277 K, and a minimum isothermal compressibility at 319 K.

The underlying reason for these anomalous characteristics is related to water's remarkable ability to form strong and directional hydrogen bonds (H-bonds). As these hydrogen bonds are constantly breaking and re-forming on a picosecond time scale, fluctuations occur in the local structure of water, leading to the emergence of water motifs (or patches) with different densities.[11,12] Today, two contrasting schools of thought seek to explain the anomalous properties of water by investigating its structural fluctuations. The continuous distribution models of water propose a homogeneous structural distribution caused by thermal fluctuations.[13−15] The two-state model, on the contrary, argues that the anomalies stem from the coexistence of two distinct preferred local structural arrangements of water molecules that have different physical properties (e.g., the density differs by ∼20%[4]): a low-density liquid (LDL) and a high-density liquid (HDL). These local structures become increasingly well-defined upon supercooling and begin to contribute around the compressibility minimum.[4,8,11,16] While LDL is an open tetrahedral configuration with predominantly low-energy H-bonds, HDL is a network with shorter and highly disordered H-bonds.[16−22]

This two-state scenario appears today to be very likely, as both theoretical[23−28] and experimental results[29−40] support the existence of a liquid−liquid critical point located in the supercooled liquid region of the water phase diagram, separating a one-phase region from a two-phase region where the LDL and HDL patches coexist, separated by a first-order transition line[4,11,41−43] (Supporting Information and Figure S1). The coexistence of these two structural motifs of water has been observed both *in silico*[41,44−46] and in experimental[21,47−53] works, especially upon supercooling. Although further experimental evidence for inhomogeneous

Received: January 4, 2024
Revised: February 14, 2024
Accepted: February 16, 2024

https://doi.org/10.1021/acs.jpclett.4c00044
J. Phys. Chem. Lett. 2024, 15, 2606−2615

structures of liquid water and fluctuations between HDL and LDL patches was provided by the isosbestic point in the temperature-dependent OH stretching Raman signal,[54,55] temperature-dependent infrared spectra of liquid water,[56] optical Kerr effect measurements,[57] and X-ray absorption and emission spectroscopy,[42,47−49,58] the coexistence of these fluctuations under ambient conditions and their implications remain elusive and controversial.[14,16,21,59−66] Nonetheless, showcasing two distinct arrangements of water molecules and their fluctuations is crucial, as it has the potential to revolutionize our understanding of biochemistry and reveal that life-supporting conditions may hinge on the presence of two kinds of H-bond organization in liquid water.[1,3,67]

Little is known about the topology of liquid water, specifically regarding the existence of motifs forming the H-bond networks such as rings, clathrates, and clusters, which, although numerically proposed through molecular dynamics,[45,68−70] have not been experimentally observed. This knowledge gap arises because techniques commonly employed to investigate density fluctuations in liquid water and H-bond network structures are limited to a length scale of ∼1 nm (Figure 1). Therefore, there is a strong demand for

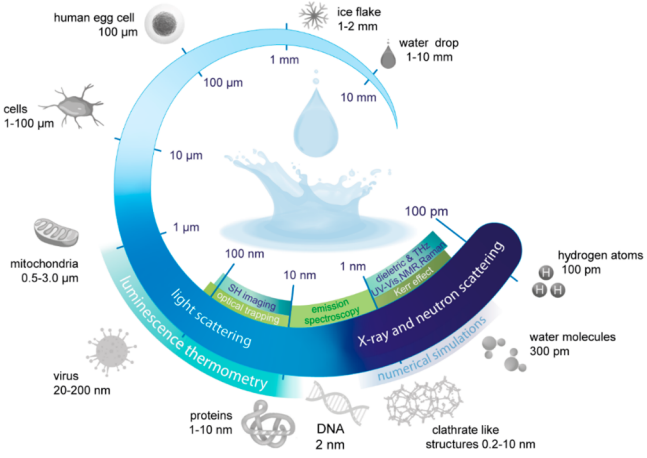

Figure 1. Infographic of the various techniques used to investigate anomalies in liquid water across different length scales. The temperature dependence of the H-bond networks has been explored at different length scales. While X-ray and neutron scattering, numerical simulations, and Kerr effect, dielectric, terahertz, ultraviolet−visible, nuclear magnetic resonance, and Raman spectroscopies operate at the length scale of hydrogen atoms and water molecules, SH imaging works at longer scales. Light scattering and luminescence nanothermometry, as shown in this work, can also be used up to a submicrometer length scale.

experimental techniques for microscopically deciphering H-bond structures in liquid water as well as in aqueous solutions of electrolytes, suspensions of biomolecules, and inorganic materials. These systems have garnered more attention due to their potential to unveil the intricate relationship among charged interfaces, high- to low-density liquid fluctuations, and their role in the formation of large-scale H-bond supramolecular structures, as suggested by molecular dynamics simulations of the hydration shell of the lysozyme protein.[71] Supramolecular structures of orientationally ordered water as large as 1 μm have been reported in light scattering measurements of aqueous solutions of low-molar mass compounds[72−74] and in wide-field second harmonic (SH) microscopy of divalent cations interacting with water and negatively charged free-standing lipid bilayers,[75,76] although not explicitly connected to HDL and LDL domains.

In recent years, there has been extensive research into the temperature dependence of the optical properties of a wide range of water-suspended materials such as quantum dots,[52] plasmonic[77] and luminescent[78] nanoparticles, organic molecules,[79−81] and trivalent lanthanide-based materials,[82−84] including upconverting nanoparticles (UCNPs).[85−87] The temperature (T) at which these materials exhibit a notable change in their optical properties is often termed the crossover temperature (T_c).[52] It predominantly falls within the range of 320−340 K and coincides with the minimum of the isothermal compressibility of water.[50] Surprisingly, although some of these measurements have been interpreted in light of the two-state model of water,[52,80] the observed bilinear trend has not been explicitly attributed to the presence of HDL and LDL motifs or the fluctuations between them. To the best of our knowledge, only one research paper has explored the intriguing relationship between the bilinear temperature dependence of the instantaneous Brownian velocity of $NaYF_4$:Yb/Er UCNPs suspended in water and the high- to low-density liquid fluctuations.[87] These experimental data, corroborated by molecular dynamics simulations, elucidated a geometric phase transition in which the LDL phase percolates below 330 K. T_c, in this context, was interpreted as the onset of fluctuations between high- and low-density liquid water.[87]

In this work, we delve into the unique ability of upconversion nanothermometry[88] to measure the temperature and pH dependence of the Brownian velocity[89] of UCNPs of varying sizes (15−106 nm in diameter) dispersed in water [so-called nanofluids (section 2 of the Supporting Information)]. We estimate an upper-temperature threshold for the liquid water density fluctuations in the region dominated by HDL domains under ambient conditions, which agrees with the value suggested in the hypothetical phase diagram of liquid water under ambient conditions (Figure S1).[4,8,11,23,31,90] We also show that increasing the pH of the nanofluids fragments the LDL domains (the LDL−HDL fluctuations become less favorable), similar to increasing the pressure in this phase diagram. Furthermore, our results provide new insights into the relative proportion of HDL and LDL motifs that coexist in the hydration water around the particle surface under ambient conditions. We find that the high- to low-density liquid fluctuations depend on the size of the suspended nanoparticle and the pH of the nanofluid. As the size increases, the relative proportion of HDL domains increases, while as the surface charge increases (controlled by pH), the relative proportion of LDL patches increases.

We measured the instantaneous Brownian velocity of 15 nm [diameter (d)] $NaGdF_4$:Yb/Er(18%/2%)@$NaGdF_4$ core−shell UCNPs dispersed in water (H_2O, pH 5.10), heavy water (D_2O), and ethanol (EtOH) at a volume fraction of 0.085% (Figure 2a and Table S1). The colloidal stability of the nanofluids and the size distribution of the UCNPs are presented in Figures S2−S6 and Table S2. The experimental setup, similar to that in ref 89, is described in sections 2 and 3 of the Supporting Information, Figures S7−S10, and Table S3. As the solvent density (ρ) increases, the Brownian velocity decreases because denser liquids have a higher effective mass (defined as the combined mass of the UCNPs and half of the liquid mass moving cooperatively with them).[91] This is well illustrated by the difference in density between EtOH and D_2O

https://doi.org/10.1021/acs.jpclett.4c00044
J. Phys. Chem. Lett. 2024, 15, 2606−2615

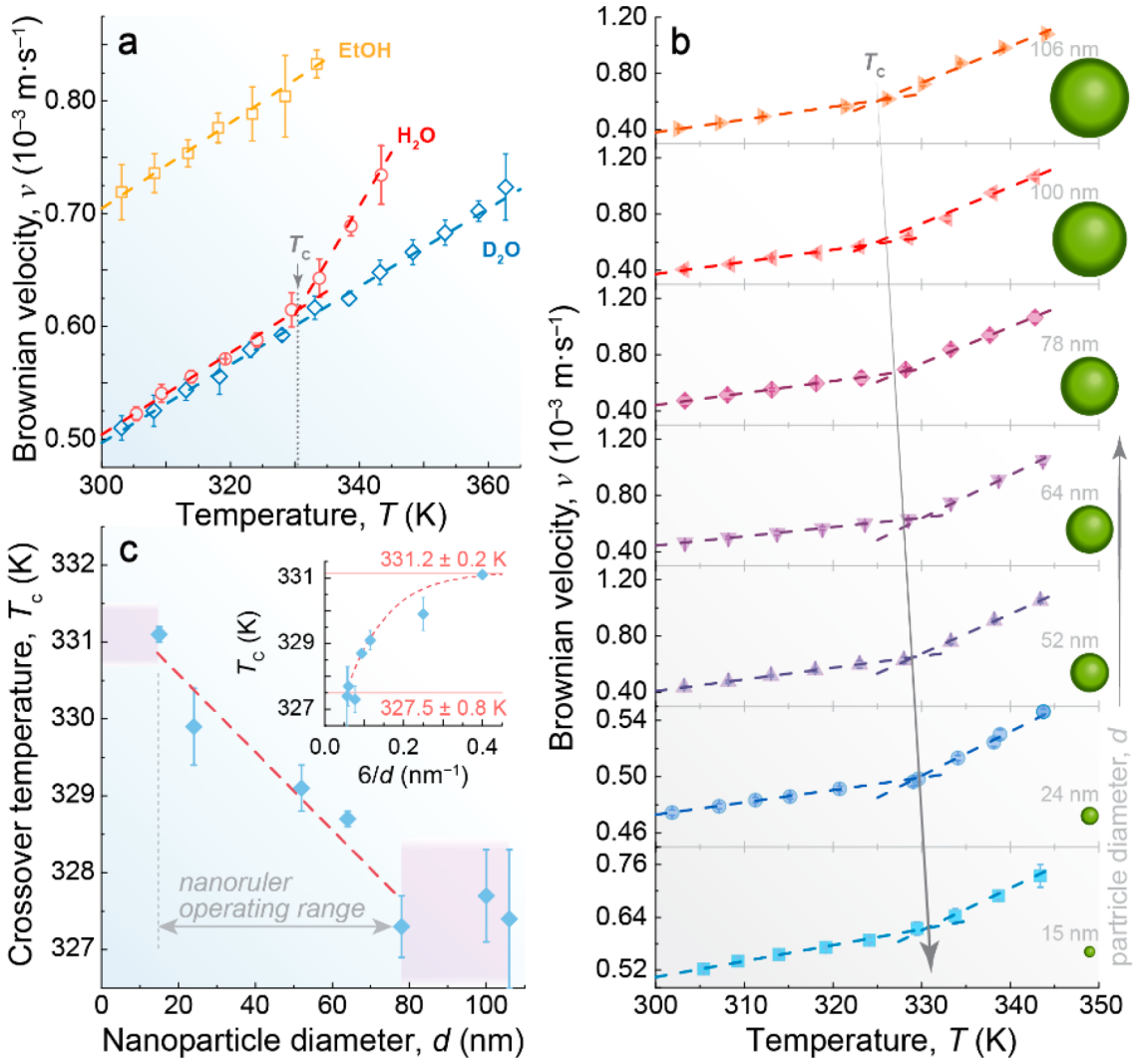

Figure 2. Solvent effect and size dependence in the Brownian velocity of UCNPs. (a) Temperature-dependent Brownian velocity of the 15 nm UCNPs suspended in EtOH, H_2O, and D_2O. The gray arrow highlights the existence of a crossover temperature in the water-suspended UCNPs around 330 K, indicating the anomalous behavior of water. (b) Temperature-dependent Brownian velocity of different-sized UCNPs (15−106 nm) at pH 5.10. (c) Size-dependent crossover temperature of the nanofluids from panel b, where the red dashed line is a guide for the eyes, highlighting the operating range of sizes that can be used to probe the different motifs of liquid water. The inset presents the dependence of T_c on the surface/volume ratio ($S/V = 6/d$). The lines are guides for the eyes.

(781 and 1105 kg m^{-3}, respectively, at 303 K[92]). The lower density of EtOH facilitates the faster motion of the UCNPs within the nanofluid, whereas the higher density of D_2O results in considerably slower motion (Figure 2a). An analogous density dependence was observed in the Brownian velocity of UCNPs containing an oleic acid coating and dispersed in toluene and cyclohexane, where the increase in solvent density decelerates the motion of particles.[87]

The Brownian velocity of the UCNPs depends on the particle size, decreasing by ∼20% when the size increases from 15 to 64 nm and being almost independent of size for larger values of ≤106 nm, as observed in Figure 2b and Figure S11a. Due to the same volume fraction used across all colloidal suspensions (0.085%), smaller particle sizes correspond to a greater number of UCNPs in the suspensions (Figure S11 and Table S4). Consequently, this results in an increased Brownian velocity of the UCNPs with a higher particle count in the suspension. The number of UCNPs increases by a factor of ∼4 when the particle size decreases from 106 to 64 nm. However, this increment is far more striking, reaching a factor of 40, when the size decreases from 52 to 15 nm. The observed decrease in Brownian velocity as UCNP size increases is therefore attributed to the dependence of Brownian velocity on the number of particles per unit of volume in the suspensions due to the particle−particle interactions. It is noteworthy that these findings align seamlessly with our earlier observations.[89]

Notably, the Brownian velocity of the UCNPs in the aqueous nanofluids exhibits a bilinear trend, regardless of the size of the particles (Figure 2b). This behavior is attributed to the presence of two distinct motion regimes for the UCNPs. When $T < T_c$ (300−330 K), there are HDL fluctuations into more voluminous LDL regions within the HDL dominant phase. Consequently, this gives rise to a greater effective mass of the nanoparticles, resulting in lower Brownian velocity values. Conversely, when the temperature exceeds the critical threshold ($T > T_c$), density fluctuations cease because all LDL motifs have already been converted into HDL ones. This leads to a liquid state characterized by localized fluctuations within

https://doi.org/10.1021/acs.jpclett.4c00044
J. Phys. Chem. Lett. 2024, 15, 2606−2615

the HDL phase, leading to higher Brownian velocity values. It is worth stressing that the obtained T_c value closely corresponds with the minimum value of the isothermal compressibility of liquid water, which is related to the change from a more to a less organized tetrahedral organization due to the density increase.[50] Once isothermal compressibility depends on fluctuations in density indicating a relative change in the volume, the similarity between the T_c values of the Brownian velocity of UCNPs and the minimum isothermal compressibility of liquid water is explained by the change in volume of the HDL and LDL motifs with an increase in temperature.[93]

Compared to liquid water, the weaker hydrogen bonds in ethanol[94] result in a continuous linear increase in the Brownian velocity of UCNPs upon heating. Although the low boiling point of EtOH limits its study at temperatures above 333 K, the lack of tetrahedral arrangements means that T_c is not expected to occur.[95] While HDL and LDL motifs have also been identified in liquid D_2O,[96,97] the presence of isotopic quantum effects generates a more ordered structure that enhances thermodynamic stability,[98,99] displacing the Widom line toward higher temperatures (4 K at ∼0 bar).[31] The melting point (4 K), maximum density (7 K), isothermal compressibility (5 K), nuclear quantum effects (5 K), and viscosity (−6.5 K) also exhibit a temperature offset in D_2O relative to the values in H_2O.[100−104] Then, T_c might be shifted by a few degrees. No crossover temperature, however, was observed in the temperature dependence of the Brownian velocity of the UCNPs in D_2O (Figure 2a).

Interestingly, recent findings on the three-dimensional confinement of light and heavy water within zwitterionic liposomes of different sizes, as determined through SH imaging and scattering experiments, have yielded a noteworthy conclusion: The H-bond networks in D_2O differ not only at subnanometer length scales but also at length scales of ≲100 nm.[76] This significantly exceeds the previously observed confinement length scales of ∼2−20 nm.[76] On the contrary, experimental[105] and simulation[106,107] results have shown that the dielectric constant of confined water is much lower than that of bulk water. Similarly, Kim et al.[108] highlighted how the confinement of interfacial water molecules caused by surface charge results in a lower dielectric constant at the hydration layer, which can be controlled by changing the temperature at the surface. Therefore, the Brownian velocity of UCNPs dispersed in heavy water displays an uninterrupted linear increase from room temperature to the boiling point, similar to the behavior observed for water at temperatures below T_c (Figure 2a), because of the much larger spatial extent over which H_2O molecules interact in the hydration water of the UCNPs, corresponding to a much larger spatial extent for low- to high-density liquid water fluctuations.

We observed a pronounced reduction in the T_c values of the nanofluids as the diameter d of the UCNPs increased (Figure 2c). This intriguing size-dependent trend shows that, as $d \rightarrow 0$, T_c converges toward 331.2 ± 0.2 K, as nicely illustrated by the surface/volume (S/V) ratio of the UCNPs [quasi-spherical morphology (Figure S5)] in the inset of Figure 2c. This temperature should therefore correspond to the onset temperature of the fluctuations between high- and low-density liquid states in pure water (d = 0 in Figure 2c). Interestingly, this upper-temperature threshold for fluctuations in the HDL domain-dominated region under ambient conditions agrees with the value (325.0 ± 1.0 K) estimated based on data from the hypothetical phase diagram of water under ambient conditions published in refs 4 and 8 (Figure 3).

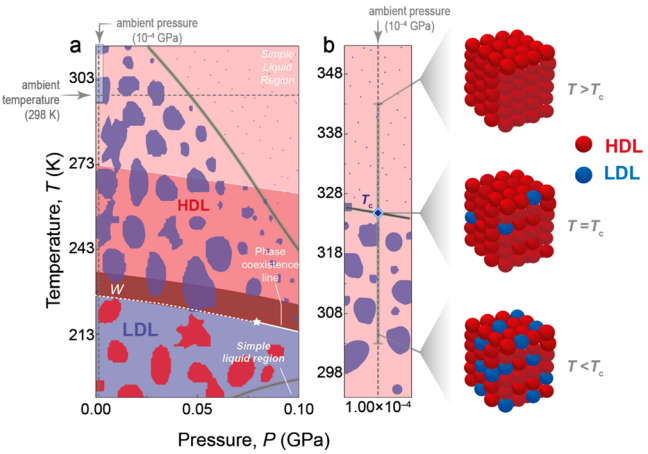

Figure 3. Hypothetical phase diagram of liquid water. (a) Coexistence of HDL (red) and LDL (blue) domains near the Widom line (W). Below W, LDL dominates with fluctuations in HDL domains, whereas above W, HDL dominates with LDL fluctuations. The white star represents the liquid−liquid critical point. With greater distance from the critical point, fluctuations decrease in size, as indicated by the blobs. The gray line outlines the "funnel of life", where water exhibits unusual properties crucial for maintaining life. Outside the funnel, at higher temperatures, only local fluctuations occur in the HDL liquid (indicated by small blue dots on the red background). Reproduced with permission from ref 8. Copyright 2019 Springer Nature. (b) Close-up of the shaded area in panel a showing the upper-temperature limit of the "funnel of life" at ambient pressure, corresponding to crossover temperature T_c (diamond), and illustrative schemes of the temperature dependence of high- to low-density liquid fluctuations.

Furthermore, we hypothesize that the decrease in the T_c of the aqueous nanofluids derived from Figure 2c compared to pure water stems from a decrease in the high- to low-density liquid water fluctuations as a consequence of the prevalence of a higher concentration of HDL patches relative to LDL regions in the volume of nanofluid moving cooperatively with UCNPs. Notably, this hypothesis corroborates previous findings, both *in silico*[71] and in experiments,[109] about the hydration water of the lysozyme protein. This hydration water (defined as the water molecules encompassing the protein within a 0.6 nm shell)[71] exhibits local distortions when compared to bulk water. For instance, its density is much higher than that of the bulk[110] and the dielectric constant of interfacial water in the double layer is much lower than that of bulk water.[108] These distortions induce a different ordering of water molecules at the interface, characterized by a higher concentration of HDL domains than LDL domains, compared to bulk water.[71,109] Like the impact of the lysozyme protein in liquid water, the presence of UCNPs also influences the local structure of water within the aqueous nanofluids. Consequently, nanofluids with larger UCNPs (lower S/V ratios) contain a relatively higher proportion of HDL domains in the hydration shell of the nanoparticles, leading to lower T_c values (Figure 2c). When d > 78 nm, T_c reaches a plateau at ∼327.5 K. This occurs because the S/V ratio changes negligibly beyond this size threshold. Remarkably, the T_c of ligand-free and silica-coated UCNPs of comparable size is similar (Figure 2c), suggesting an analogous relative HDL/LDL proportion at the particle surface, in agreement with an identical charge density of the

https://doi.org/10.1021/acs.jpclett.4c00044
J. Phys. Chem. Lett. 2024, 15, 2606−2615

water−silica and water $NaYF_4$ interfaces [$|\zeta| \sim 35$ mV (Figures S3 and S4)].

The vicinity of the UCNPs can be sensitively influenced by local ions and ligands, with effects already occurring at extremely low concentrations.[111] Fine-tuning the pH of suspensions at the water−silica interface was found to induce changes in charge density, impacting the orientation of water molecules.[110,112] Recent surface-enhanced IR absorption spectroscopy results have also shed light on the influence of pH on hydrogen and water binding energies on platinum surfaces.[113] Also, a pH dependence of the onset temperature of the anomaly related to the minimum isothermal compressibility of liquid water was reported for aqueous suspensions, including 1-methyl-5-nitroindoline,[80] Eu^{3+} complexes,[82,83] and $NaYF_4$:Yb/Er UCNPs.[86] These findings suggest a potential role of pH in influencing high- to low-density fluctuations within aqueous nanofluids.

To explore this possibility, we evaluated the temperature-dependent Brownian velocity of the UCNPs dispersed in aqueous nanofluids while systematically varying the pH values from 2.70 to 8.50 (Figure 4a for d values of 15, 64, and 78 nm

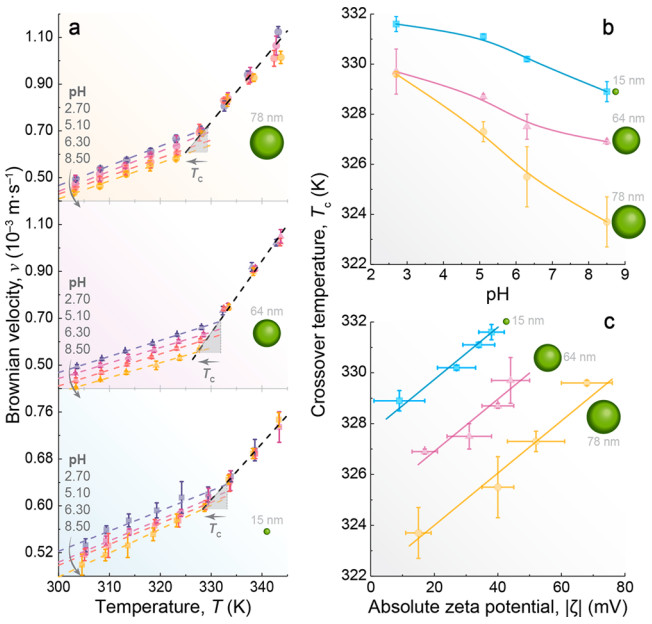

Figure 4. Correlation among the crossover temperature, pH, and ζ potential. (a) Effect of pH on the Brownian velocity of UCNPs with diameters within the operating range of the nanorulers, as defined in Figure 2c. The dashed lines are the best linear fits at each pH for $T < T_c$ and the same linear fit for all of the pH values for $T > T_c$ ($r^2 > 0.98$ for all samples). T_c as a function of (b) pH and (c) $|\zeta|$. The solid lines are guides to the eyes.

and Figure S12 for d values of 24, 52, and 106 nm). Except for pH values between 7.0 and 8.0, the measured absolute ζ potential values ($|\zeta| > 20$ mV) indicate stability with no UCNP aggregation (Figures S3 and S4).

pH exerts a notable influence on Brownian velocity, with an increase in pH leading to a reduction in Brownian velocity when $T < T_c$, while the pH dependence becomes negligible when $T > T_c$. This impact is primarily on LDL domains, present only when $T < T_c$. Increasing the pH weakens the H-bond network due to an increased concentration of OH^- ions, disrupting the tetrahedral organization of LDL domains due to their voluminous planar structure.[114] Increasing the pH triggers the fragmentation of LDL domains into smaller ones,[8] while keeping the HDL/LDL ratio, leading to a deceleration of the motion of the UCNPs. This effect mirrors the application of high pressures, as suggested by previous neutron diffraction measurements[114,115] and Monte Carlo simulations.[116] As the pressure increases at a constant temperature, the LDL−HDL fluctuations become less favorable.[8] This can be visualized as the fragmentation of the LDL domains (Figure 3 and Figure S1). However, recent machine learning-based molecular dynamics simulations of ions in salt water have shown that the ions do not homogeneously distort the structure of water but instead have localized structural effects in the first solvation shell.[117] Our results agree with this scenario as increasing the pH of the nanofluids is an ingenious strategy for simulating a pressure-like effect and evaluating microscopic changes in H-bond networks.

The decrease in Brownian velocity with an increase in pH results in a concomitant decrease in T_c values (Figure 4b), indicating that low- to high-density liquid fluctuations at nanoparticle surfaces cease at lower temperatures in basic media compared to acidic media. To explain this dependence, we consider the influence of pH on the surface charge of UCNPs, with experiments demonstrating how surface charge controls the water structure near the interface. The fine-tuning of pH affects the extent of orientation of water molecules near the interface, as reported for water−silica interfaces.[108,110] Therefore, to study the effect of pH on the electric double layer of UCNPs, we measured the ζ potential of the distinct aqueous nanofluids. Our results show a decrease in $|\zeta|$ as pH increases (Figure S4), in good accordance with previous reports on upconverting[118] and plasmonic[111] nanoparticles. This mirrors the trend observed for T_c (Figure 4b and Figure S13), highlighting how the presence of ions in the medium can affect the surface charge of the UCNPs. The increase in the extent of electrostatic repulsion of the UCNPs causes a higher T_c value (Figure 4c). As higher T_c values correspond to larger amounts of LDL patches, as discussed above, we propose that a greater surface charge (or the electrical potential at the slipping plane) increases the proportion of LDL patches in the hydration water of the nanoparticles. This hypothesis agrees with simulations conducted by Gallo's group, indicating a slower decrease in the rate of LDL domains at the biomolecule interface with an increase in temperature.[71] Moreover, for a constant $|\zeta|$ value, nanofluids with smaller UCNPs exhibit a higher T_c, consistent with the findings depicted in Figure 2c. It is noteworthy that the same conclusion can be drawn exclusively from upconversion thermometry and by combining upconversion thermometry with ζ potential measurements. Similar results were reported by Kim et al.,[108] demonstrating how temperature changes the interfacial structure of water by mitigating the effect of surface charge at water−oil interfaces.

Interestingly, Barisik et al.[119] showed that, at a constant pH, the surface charge density of Si-NPs decreases with an increase in particle size until it stabilizes after reaching a critical diameter of 100 nm. A similar trend was observed for metal oxide nanoparticles.[120] These findings align with our T_c size dependence results (Figure 2c), revealing a decrease in T_c with an increase in particle size up to a critical value (>78 nm), beyond which it remains constant.

In summary, our study systematically investigated the impact of temperature and pH on Brownian velocity in a range of UCNPs (15−106 nm diameter) dispersed in water. We

https://doi.org/10.1021/acs.jpclett.4c00044
J. Phys. Chem. Lett. 2024, 15, 2606−2615

consistently observed a decrease in the onset temperature of high- to low-density liquid water fluctuations with an increase in nanoparticle size, indicative of an increased presence of HDL domains at nanoparticle surfaces. UCNPs, therefore, behave as nanorulers for assessing the HDL/LDL proportion in surrounding hydration water. Moreover, the upper-temperature threshold for these fluctuations, as predicted by our experiments, agrees with values proposed in the hypothetical phase diagram of water under ambient conditions based on the two-state model. Additionally, we have shown that increasing the pH decreases T_c and decreasing the T_c decreases the relative amount of LDL patches, akin to external pressure on pure water. By precisely controlling the UCNP size and pH levels, we have simulated the effects of temperature and pressure on HDL and LDL hydrogen bonding networks, mirroring predictions in the hypothesized phase diagram. Within nanofluids, the local environment around nanoparticles exerts a significant influence on their physical−chemical properties, being different from the bulk due to interaction with the particle surface.[111] This work elegantly underscores the substantial impact of these interactions, serving as compelling evidence of this effect for a specific example of luminescent nanoparticles.

These findings resonate with the intricate interplay between water and various nonpolar media, metals, oxides, and biomembranes, emphasizing the importance of the water charge-asymmetrical molecular configuration at interfaces.[75,108,110] In conclusion, our results provide compelling experimental evidence regarding the significance of the size of suspended nanoparticles or biomolecules in understanding the dynamics of high- to low-density liquid fluctuations and water behavior at charged interfaces.

METHODS

Synthesis of Upconverting Nanoparticles. $NaGdF_4$:Yb/Er(18/2%)@$NaGdF_4$ (average diameter of 15 nm, core−shell), $NaYF_4$:Yb/Er(18/2%)@$NaYF_4$ (average diameter of 24 nm, core−shell), $NaYF_4$:Lu/Yb/Er(40/18/2%) (average diameter of 52 nm, core-only), $NaYF_4$:Lu/Yb/Er(47/18/2%) (average diameter of 64 nm, core-only), $NaYF_4$:Lu/Yb/Er(47/18/2%) (average diameter of 78 nm, core-only), $NaYF_4$:Lu/Yb/Er(47/18/2%)@SiO_2 (average diameter of 100 nm, core−shell), and $NaYF_4$:Lu/Yb/Er(50/18/2%) (average diameter of 106 nm, core-only) ligand-free UCNPs were synthesized through a coprecipitation method based on a previous report.[121] The detailed synthesis procedure and the characterization of the UCNPs are described in section 2 of the Supporting Information.

Preparation of the Nanofluids. Aqueous nanofluids containing ligand-free UCNPs were obtained by adjusting the pH of water between 2.70 and 5.10 by adding aqueous solutions of sodium hydroxide and hydrochloric acid (0.1 mol L^{-1}) at a volume fraction (ϕ) of 0.085%. The aqueous nanofluids of 15 nm UCNPs were freeze-dried, and the resulting powder was dispersed in heavy water and ethanol under sonication to obtain the corresponding nanofluids at ϕ = 0.085%. A detailed description of pH measurements and the preparation of nanofluids is presented in section 2 of the Supporting Information.

Upconversion Spectroscopy. The upconverting emission spectra of the nanofluids were recorded using the experimental setup shown in Figure S7. A quartz cuvette (9F-Q-10, Starna Cells) filled with 0.50 mL of the nanofluids was irradiated with a near-infrared 980 nm laser diode (DL980-3W0-T, CrystaLaser) operating with a power density (P_D) of 62 W cm^{-2}. The excitation radiation was collimated with a plano-convex lens (LA1145-AB, Thorlabs). The upconversion emission spectra were registered with a USB portable spectrometer (Maya 2000 Pro, Ocean Insight) coupled to an optical fiber (P600-1-UV-vis, Ocean Insight). A short pass filter (FESH0750, Thorlabs) was used to cut off the 980 nm laser signal from the emission spectra. The temperature of the nanofluids was increased through the Joule effect by attaching a Kapton thermofoil heater (HK6906, Minco) in thermal contact with one side of the cuvette containing the nanofluids. This setup allows us to control both the initial temperature and the temperature increase. Further information is provided in section 2 of the Supporting Information.

Measurement of Temperature through Upconversion Nanothermometry. The luminescence intensity ratio between the emission bands corresponding to the Er^{3+} $^2H_{11/2} \rightarrow {}^4I_{15/2}$ (I_H, 510−534 nm) and $^4S_{3/2} \rightarrow {}^4I_{15/2}$ (I_S, 534−554 nm) transitions was used to define a thermometric parameter ($\Delta = I_H/I_S$) and predict absolute temperature T of the nanofluids as detailed in section 3 of the Supporting Information.

Determination of the Brownian Velocity of the UCNPs in the Nanofluids. The emission spectra were recorded at different distances x_i from the Kapton thermofoil heater to construct time-dependent temperature profiles through upconversion nanothermometry. An excellent linear correlation between x_i and the onset time (the time at which the temperature increases above its uncertainty) was systematically obtained. The slope of the linear fit to each data set represents the Brownian velocity of the UCNPs in the nanofluids. Further details are provided in sections 4−6 of the Supporting Information.

ASSOCIATED CONTENT

Supporting Information

The Supporting Information is available free of charge at https://pubs.acs.org/doi/10.1021/acs.jpclett.4c00044.

Description of the two-state model and a hypothetical phase diagram of liquid water, nanoparticle synthesis, characterization of materials, and a study of the thermometric performance and an investigation of the instantaneous Brownian velocity of upconverting nanoparticles (PDF)

Transparent Peer Review report available (PDF)

AUTHOR INFORMATION

Corresponding Authors

Xiaogang Liu − *Department of Chemistry, National University of Singapore, Singapore 117543;* orcid.org/0000-0003-2517-5790; Email: chmlx@nus.edu.sg

Luís D. Carlos − *Phantom-g, CICECO - Aveiro Institute of Materials, Department of Physics, University of Aveiro, 3810-193 Aveiro, Portugal;* orcid.org/0000-0003-4747-6535; Email: lcarlos@ua.pt

Authors

Fernando E. Maturi − *Phantom-g, CICECO - Aveiro Institute of Materials, Department of Physics, University of Aveiro, 3810-193 Aveiro, Portugal; Institute of Chemistry, São Paulo State University (UNESP), 14800-060 Araraquara, SP, Brazil;* orcid.org/0000-0002-9305-8185

https://doi.org/10.1021/acs.jpclett.4c00044
J. Phys. Chem. Lett. 2024, 15, 2606−2615

Ramon S. Raposo Filho − *Phantom-g, CICECO - Aveiro Institute of Materials, Department of Physics, University of Aveiro, 3810-193 Aveiro, Portugal*

Carlos D. S. Brites − *Phantom-g, CICECO - Aveiro Institute of Materials, Department of Physics, University of Aveiro, 3810-193 Aveiro, Portugal;* orcid.org/0000-0001-9636-2628

Jingyue Fan − *Department of Chemistry, National University of Singapore, Singapore 117543;* orcid.org/0000-0003-4987-7025

Ruihua He − *Department of Chemistry, National University of Singapore, Singapore 117543*

Bilin Zhuang − *Harvey Mudd College, Claremont, California 91711, United States;* orcid.org/0000-0003-2934-4264

Complete contact information is available at: https://pubs.acs.org/10.1021/acs.jpclett.4c00044

Notes

The authors declare no competing financial interest.

■ ACKNOWLEDGMENTS

This work was partially developed within the scope of Project CICECO-Aveiro Institute of Materials, UIDB/50011/2020 (DOI 10.54499/UIDB/50011/2020), UIDP/50011/2020 (DOI 10.54499/UIDP/50011/2020), and LA/P/0006/2020 (DOI 10.54499/LA/P/0006/2020), financed by national funds through the FCT/MCTES (PIDDAC). This work was also financially supported by the project *Shape of Water* (PTDC/NAN-PRO/3881/2020) through Portuguese funds. F.E.M. acknowledges funding from the European Union's Horizon 2020 research and innovation program under Marie Sklodowska-Curie Grant Agreement 823941 (FUNGLASS) and financial support from the FCT through Grant UI/BD/151445/2021. The authors thank Ricardo Longo (Federal University of Pernambuco), Christoph Rose-Petruck (Brown University), and Artemov Vasily (EPFL) for fruitful discussions.

■ REFERENCES

(1) Chaplin, M. Do we underestimate the importance of water in cell biology? *Nat. Rev. Mol. Cell Bio.* **2006**, *7* (11), 861−866.
(2) Ball, P. Water - an enduring mystery. *Nature* **2008**, *452* (7185), 291−292.
(3) Pohorille, A.; Pratt, L. R. Is water the universal solvent for life? *Orig. Life Evol. Biosph.* **2012**, *42*, 405−409.
(4) Gallo, P.; Amann-Winkel, K.; Angell, C. A.; et al. Water: A tale of two liquids. *Chem. Rev.* **2016**, *116* (13), 7463−7500.
(5) Bellissent-Funel, M. C.; Hassanali, A.; Havenith, M.; et al. Water determines the structure and dynamics of proteins. *Chem. Rev.* **2016**, *116* (13), 7673−7697.
(6) Brini, E.; Fennell, C. J.; Fernandez-Serra, M.; Hribar-Lee, B.; Luksic, M.; Dill, K. A. How water's properties are encoded in its molecular structure and energies. *Chem. Rev.* **2017**, *117* (19), 12385−12414.
(7) Ball, P. Water is an active matrix of life for cell and molecular biology. *Proc. Natl. Acad. Sci. U.S.A.* **2017**, *114* (51), 13327−13335.
(8) Pettersson, L. G. M. A two-state picture of water and the funnel of life. In *Modern Problems of the Physics of Liquid Systems*; Springer Proceedings in Physics, 2019; pp 3−39.
(9) Errington, J. R.; Debenedetti, P. G. Relationship between structural order and the anomalies of liquid water. *Nature* **2001**, *409* (6818), 318−321.
(10) Chaplin, M. Water structure and science. https://water.lsbu.ac.uk/water/water_structure_science.html (accessed 2024-06-02).
(11) Nilsson, A.; Pettersson, L. G. M. The structural origin of anomalous properties of liquid water. *Nat. Commun.* **2015**, *6* (1), 8998.
(12) Russo, J.; Akahane, K.; Tanaka, H. Water-like anomalies as a function of tetrahedrality. *Proc. Natl. Acad. Sci. U.S.A.* **2018**, *115* (15), 3333−3341.
(13) Clark, G. N. I.; Hura, G. L.; Teixeira, J.; Soper, A. K.; Head-Gordon, T. Small-angle scattering and the structure of ambient liquid water. *Proc. Natl. Acad. Sci. U.S.A.* **2010**, *107* (32), 14003−14007.
(14) Soper, A. K. Is water one liquid or two? *J. Chem. Phys.* **2019**, *150* (23), 234503.
(15) Niskanen, J.; Fondell, M.; Sahle, C. J.; et al. Compatibility of quantitative X-ray spectroscopy with continuous distribution models of water at ambient conditions. *Proc. Natl. Acad. Sci. U.S.A.* **2019**, *116* (10), 4058−4063.
(16) Huang, C.; Wikfeldt, K. T.; Tokushima, T.; et al. The inhomogeneous structure of water at ambient conditions. *Proc. Natl. Acad. Sci. U.S.A.* **2009**, *106* (36), 15214−15218.
(17) Soper, A. K.; Ricci, M. A. Structures of high-density and low-density water. *Phys. Rev. Lett.* **2000**, *84* (13), 2881−2884.
(18) Mallamace, F.; Corsaro, C.; Stanley, H. E. Possible relation of water structural relaxation to water anomalies. *Proc. Natl. Acad. Sci. USA* **2013**, *110* (13), 4899−4904.
(19) Shi, R.; Russo, J.; Tanaka, H. Common microscopic structural origin for water's thermodynamic and dynamic anomalies. *J. Chem. Phys.* **2018**, *149* (22), 224502.
(20) Lin, C.; Smith, J. S.; Sinogeikin, S. V.; Shen, G. Experimental evidence of low-density liquid water upon rapid decompression. *Proc. Natl. Acad. Sci. U.S.A.* **2018**, *115* (9), 2010−2015.
(21) Shi, R.; Tanaka, H. Direct evidence in the scattering function for the coexistence of two types of local structures in liquid water. *J. Am. Chem. Soc.* **2020**, *142* (6), 2868−2875.
(22) Oka, K.; Shibue, T.; Sugimura, N.; Watabe, Y.; Tanaka, M.; Winther-Jensen, B.; Nishide, H. Two states of water converge to one state below 215 k. *J. Phys. Chem. Lett.* **2021**, *12* (24), 5802−5806.
(23) Poole, P. H.; Sciortino, F.; Essmann, U.; Stanley, H. E. Phase-behavior of metastable water. *Nature* **1992**, *360* (6402), 324−328.
(24) Palmer, J. C.; Martelli, F.; Liu, Y.; Car, R.; Panagiotopoulos, A. Z.; Debenedetti, P. G. Metastable liquid−liquid transition in a molecular model of water. *Nature* **2014**, *510* (7505), 385−388.
(25) Palmer, J. C.; Poole, P. H.; Sciortino, F.; Debenedetti, P. G. Advances in computational studies of the liquid-liquid transition in water and water-like models. *Chem. Rev.* **2018**, *118* (18), 9129−9151.
(26) Debenedetti, P. G.; Sciortino, F.; Zerze, G. H. Second critical point in two realistic models of water. *Science* **2020**, *369* (6501), 289−292.
(27) Weis, J.; Sciortino, F.; Panagiotopoulos, A. Z.; Debenedetti, P. G. Liquid-liquid criticality in the wail water model. *J. Chem. Phys.* **2022**, *157* (2), 024502.
(28) Yu, Z. H.; Shi, R.; Tanaka, H. A unified description of the liquid structure, static and dynamic anomalies, and criticality of TIP4P/2005 water by a hierarchical two-state model. *J. Phys. Chem. B* **2023**, *127* (15), 3452−3462.
(29) Angell, C. A. Insights into phases of liquid water from study of its unusual glass-forming properties. *Science* **2008**, *319* (5863), 582−587.
(30) Angell, C. A. Supercooled water two phases? *Nat. Mater.* **2014**, *13* (7), 673−675.
(31) Kim, K. H.; Spah, A.; Pathak, H.; et al. Maxima in the thermodynamic response and correlation functions of deeply supercooled water. *Science* **2017**, *358* (6370), 1589−1593.
(32) Gallo, P.; Stanley, H. E. Experiments provide evidence for two liquid phases in supercooled water droplets. *Science* **2017**, *358* (6370), 1543−1544.
(33) Handle, P. H.; Loerting, T.; Sciortino, F. Supercooled and glassy water: Metastable liquid(s), amorphous solid(s), and a no-man's land. *Proc. Natl. Acad. Sci. U.S.A.* **2017**, *114* (51), 13336−13344.

(34) Woutersen, S.; Ensing, B.; Hilbers, M.; Zhao, Z.; Angell, C. A. A liquid-liquid transition in supercooled aqueous solution related to the HDA-LDA transition. *Science* **2018**, *359* (6380), 1127−1131.
(35) Kringle, L.; Thornley, W. A.; Kay, B. D.; Kimmel, G. A. Reversible structural transformations in supercooled liquid water from 135 to 245 K. *Science* **2020**, *369* (6510), 1490−1492.
(36) Kim, K. H.; Amann-Winkel, K.; Giovambattista, N.; et al. Experimental observation of the liquid-liquid transition in bulk supercooled water under pressure. *Science* **2020**, *370* (6519), 978−982.
(37) Gallo, P.; Bachler, J.; Bove, L. E.; et al. Advances in the study of supercooled water. *Eur. Phys. J. E* **2021**, *44*, 143.
(38) Suzuki, Y. Direct observation of reversible liquid-liquid transition in a trehalose aqueous solution. *Proc. Natl. Acad. Sci. U.S.A.* **2022**, *119* (5), No. e2113411119.
(39) Amann-Winkel, K.; Kim, K. H.; Giovambattista, N.; et al. Liquid-liquid phase separation in supercooled water from ultrafast heating of low-density amorphous ice. *Nat. Commun.* **2023**, *14* (1), 442.
(40) Kruger, C. R.; Mowry, N. J.; Bongiovanni, G.; Drabbels, M.; Lorenz, U. J. Electron diffraction of deeply supercooled water in no man's land. *Nat. Commun.* **2023**, *14* (1), 2812.
(41) Russo, J.; Tanaka, H. Understanding water's anomalies with locally favoured structures. *Nat. Commun.* **2014**, *5* (1), 3556.
(42) Amann-Winkel, K.; Bellissent-Funel, M. C.; Bove, L. E.; Loerting, T.; Nilsson, A.; Paciaroni, A.; Schlesinger, D.; Skinner, L. X-ray and neutron scattering of water. *Chem. Rev.* **2016**, *116* (13), 7570−7589.
(43) Hamm, P. Markov state model of the two-state behaviour of water. *J. Chem. Phys.* **2016**, *145* (13), 134501.
(44) Martelli, F. Unravelling the contribution of local structures to the anomalies of water: The synergistic action of several factors. *J. Chem. Phys.* **2019**, *150* (9), 094506.
(45) Gao, Y. T.; Fang, H. W.; Ni, K.; Feng, Y. X. Water clusters and density fluctuations in liquid water based on extended hierarchical clustering methods. *Sci. Rep.* **2022**, *12* (1), 8036.
(46) de Oliveira, P. M. C.; de Souza, J. I. R.; da Silva, J. A. B.; Longo, R. L. Temperature dependence of hydrogen bond networks of liquid water: Thermodynamic properties and structural heterogeneity from topological descriptors. *J. Phys. Chem. B* **2023**, *127* (10), 2250−2257.
(47) Wernet, P.; Nordlund, D.; Bergmann, U.; et al. The structure of the first coordination shell in liquid water. *Science* **2004**, *304* (5673), 995−999.
(48) Tokushima, T.; Harada, Y.; Takahashi, O.; Senba, Y.; Ohashi, H.; Pettersson, L. G. M.; Nilsson, A.; Shin, S. High resolution X-ray emission spectroscopy of liquid water: The observation of two structural motifs. *Chem. Phys. Lett.* **2008**, *460* (4), 387−400.
(49) Harada, Y.; Tokushima, T.; Horikawa, Y.; et al. Selective probing of the oh or od stretch vibration in liquid water using resonant inelastic soft-X-ray scattering. *Phys. Rev. Lett.* **2013**, *111* (19), 193001.
(50) Skinner, L. B.; Benmore, C. J.; Neuefeind, J. C.; Parise, J. B. The structure of water around the compressibility minimum. *J. Chem. Phys.* **2014**, *141* (21), 214507.
(51) Sellberg, J. A.; Huang, C.; McQueen, T. A.; et al. Ultrafast X-ray probing of water structure below the homogeneous ice nucleation temperature. *Nature* **2014**, *510* (7505), 381−384.
(52) Maestro, L. M.; Marques, M. I.; Camarillo, E.; et al. On the existence of two states in liquid water: Impact on biological and nanoscopic systems. *Int. J. Nanotechnol.* **2016**, *13* (8), 667−677.
(53) Stern, J. N.; Seidl-Nigsch, M.; Loerting, T. Evidence for high-density liquid water between 0.1 and 0.3 GPa near 150 K. *Proc. Natl. Acad. Sci. U.S.A.* **2019**, *116* (19), 9191−9196.
(54) Sun, Q. Local statistical interpretation for water structure. *Chem. Phys. Lett.* **2013**, *568*−*569*, 90−94.
(55) Morawietz, T.; Marsalek, O.; Pattenaude, S. R.; Streacker, L. M.; Ben-Amotz, D.; Markland, T. E. The interplay of structure and dynamics in the Raman spectrum of liquid water over the full frequency and temperature range. *J. Phys. Chem. Lett.* **2018**, *9* (4), 851−857.
(56) Maréchal, Y. The molecular structure of liquid water delivered by absorption spectroscopy in the whole IR region completed with thermodynamics data. *J. Mol. Struct.* **2011**, *1004* (1), 146−155.
(57) Taschin, A.; Bartolini, P.; Eramo, R.; Righini, R.; Torre, R. Evidence of two distinct local structures of water from ambient to supercooled conditions. *Nat. Commun.* **2013**, *4* (1), 2401.
(58) Zhovtobriukh, I.; Besley, N. A.; Fransson, T.; Nilsson, A.; Pettersson, L. G. M. Relationship between X-ray emission and absorption spectroscopy and the local H-bond environment in water. *J. Chem. Phys.* **2018**, *148* (14), 144507.
(59) Pettersson, L. G. M.; Harada, Y.; Nilsson, A. Do X-ray spectroscopies provide evidence for continuous distribution models of water at ambient conditions? *Proc. Natl. Acad. Sci. U.S.A.* **2019**, *116* (35), 17156−17157.
(60) Niskanen, J.; Fondell, M.; Sahle, C. J.; et al. Reply to pettersson et al.: Why X-ray spectral features are compatible to continuous distribution models in ambient water. *Proc. Natl. Acad. Sci. U.S.A.* **2019**, *116* (35), 17158−17159.
(61) Caupin, F.; Holten, V.; Qiu, C.; Guillerm, E.; Wilke, M.; Frenz, M.; Teixeira, J.; Soper, A. K. Comment on ″Maxima in the thermodynamic response and correlation functions of deeply supercooled water. *Science* **2018**, *360* (6390), No. eaat1634.
(62) Kim, K. H.; Spah, A.; Pathak, H.; et al. Response to comment on ″Maxima in the thermodynamic response and correlation functions of deeply supercooled water. *Science* **2018**, *360* (6390), No. eaat1729.
(63) Limmer, D. T.; Chandler, D. The putative liquid-liquid transition is a liquid-solid transition in atomistic models of water. *J. Chem. Phys.* **2011**, *135* (13), 134503.
(64) Limmer, D. T.; Chandler, D. The putative liquid-liquid transition is a liquid-solid transition in atomistic models of water. II. *J. Chem. Phys.* **2013**, *138* (21), 214504.
(65) Palmer, J. C.; Haji-Akbari, A.; Singh, R. S.; Martelli, F.; Car, R.; Panagiotopoulos, A. Z.; Debenedetti, P. G. Comment on ″The putative liquid-liquid transition is a liquid-solid transition in atomistic models of water″ [I and II: J. Chem. Phys. 135. *J. Chem. Phys.* **2018**, *148* (13), 137101.
(66) Naserifar, S.; Goddard, W. A. Liquid water is a dynamic polydisperse branched polymer. *Proc. Natl. Acad. Sci. U.S.A.* **2019**, *116* (6), 1998−2003.
(67) Wiggins, P. Life depends upon two kinds of water. *PLoS One* **2008**, *3* (1), No. e1406.
(68) Camisasca, G.; Schlesinger, D.; Zhovtobriukh, I.; Pitsevich, G.; Pettersson, L. G. M. A proposal for the structure of high- and low-density fluctuations in liquid water. *J. Chem. Phys.* **2019**, *151* (3), 034508.
(69) Ansari, N.; Dandekar, R.; Caravati, S.; Sosso, G. C.; Hassanali, A. High and low density patches in simulated liquid water. *J. Chem. Phys.* **2018**, *149* (20), 204507.
(70) Neophytou, A.; Chakrabarti, D.; Sciortino, F. Topological nature of the liquid−liquid phase transition in tetrahedral liquids. *Nat. Phys.* **2022**, *18* (10), 1248−1253.
(71) Camisasca, G.; Tenuzzo, L.; Gallo, P. Protein hydration water: Focus on low density and high density local structures upon cooling. *J. Mol. Liq.* **2023**, *370*, 120962.
(72) Sedlák, M. Large-scale supramolecular structure in solutions of low molar mass compounds and mixtures of liquids: I. Light scattering characterization. *J. Phys. Chem. B* **2006**, *110* (9), 4329−4338.
(73) Sedlák, M.; Rak, D. Large-scale inhomogeneities in solutions of low molar mass compounds and mixtures of liquids: Supramolecular structures or nanobubbles? *J. Phys. Chem. B* **2013**, *117* (8), 2495−504.
(74) Sedlák, M. Large-scale supramolecular structure in solutions of low molar mass compounds and mixtures of liquids. III. Correlation with molecular properties and interactions. *J. Phys. Chem. B* **2006**, *110* (28), 13976−13984.

https://doi.org/10.1021/acs.jpclett.4c00044
J. Phys. Chem. Lett. 2024, 15, 2606−2615

(75) Tarun, O. B.; Okur, H. I.; Rangamani, P.; Roke, S. Transient domains of ordered water induced by divalent ions lead to lipid membrane curvature fluctuations. *Commun. Chem.* **2020**, *3* (1), 17.
(76) Dupertuis, N.; Tarun, O. B.; Lutgebaucks, C.; Roke, S. Three-dimensional confinement of water: H_2O exhibits long-range (> 50 nm) structure while D_2O does not. *Nano Lett.* **2022**, *22* (18), 7394−7400.
(77) del Valle, J. C.; Camarillo, E.; Martinez Maestro, L.; et al. Dielectric anomalous response of water at 60 °C. *Philos. Mag.* **2015**, *95* (7), 683−690.
(78) Munoz-Ortiz, T.; Abiven, L.; Marin, R.; et al. Temperature dependence of water absorption in the biological windows and its impact on the performance of Ag_2S luminescent nanothermometers. *Part. Part. Syst. Charact.* **2022**, *39* (11), 2200100.
(79) Catalan, J.; Gonzalo, J. A. Liquid water changes its structure at 43 °C. *Chem. Phys. Lett.* **2017**, *679*, 86−89.
(80) Catalan, J.; del Valle, J. C. Molecule 1-methyl-5-nitroindoline probes the structural change of liquid water with temperature. *ACS Omega* **2018**, *3* (12), 18930−18934.
(81) Cheng, Y.-H.; Yang, H.-C.; Chou, P.-T. Could chemical reaction at the molecular level show distinction between two liquid-water states? Study of the excited-state water-catalyzed proton transfer reaction provides a clue. *J. Phys. Chem. Lett.* **2020**, *11* (21), 9468−9475.
(82) Labrador-Páez, L.; Montes, E.; Pedroni, M.; Haro-González, P.; Bettinelli, M.; Jaque, D.; Garcia-Solé, J.; Jaque, F. Effect of H_2o and D_2o thermal anomalies on the luminescence of Eu^{3+} aqueous complexes. *J. Phys. Chem. C* **2018**, *122* (26), 14838−14845.
(83) Labrador-Páez, L.; Mingoes, C.; Jaque, F.; Haro-González, P.; Bazin, H.; Zwier, J. M.; Jaque, D.; Hildebrandt, N. pH dependence of water anomaly temperature investigated by Eu(III) cryptate luminescence. *Anal. Bioanal. Chem.* **2020**, *412*, 73−80.
(84) Labrador-Páez, L.; Kostiv, U.; Widengren, J.; Liu, H. C. Water: An influential agent for lanthanide-doped luminescent nanoparticles in nanomedicine. *Adv. Opt. Mater.* **2023**, *11* (11), 2200513.
(85) Labrador-Páez, L.; Jovanović, D. J.; Marqués, M. I.; et al. Unveiling molecular changes in water by small luminescent nanoparticles. *Small* **2017**, *13* (30), 1700968.
(86) Lu, D. S.; Labrador-Páez, L.; Ortiz-Rivero, E.; et al. Exploring single-nanoparticle dynamics at high temperature by optical tweezers. *Nano Lett.* **2020**, *20* (11), 8024−8031.
(87) Brites, C. D. S.; Zhuang, B. L.; Debasu, M. L.; et al. Decoding a percolation phase transition of water at ∼ 330 K with a nanoparticle ruler. *J. Phys. Chem. Lett.* **2020**, *11* (16), 6704−6711.
(88) Brites, C. D. S.; Marin, R.; Suta, M.; Carneiro Neto, A. N.; Ximendes, E.; Jaque, D.; Carlos, L. D. Spotlight on luminescence thermometry: Basics, challenges, and cutting-edge applications. *Adv. Mater.* **2023**, *35* (36), 2302749.
(89) Brites, C. D.; Xie, X.; Debasu, M. L.; et al. Instantaneous ballistic velocity of suspended brownian nanocrystals measured by upconversion nanothermometry. *Nat. Nanotechnol.* **2016**, *11* (10), 851−856.
(90) Stanley, H. E. Mysteries of water. In *Hydration processes in biology: Theoretical and experimental approaches, Proceedings of the NATO advanced study institute*; Bellissent-Funel, M.-C., Ed.; IOS Press: Amsterdam, 1999; Vol. *305*.
(91) Huang, R. X.; Chavez, I.; Taute, K. M.; Lukic, B.; Jeney, S.; Raizen, M. G.; Florin, E. L. Direct observation of the full transition from ballistic to diffusive Brownian motion in a liquid. *Nat. Phys.* **2011**, *7* (7), 576−580.
(92) Haynes, W. M.; Lide, D. R. *CRC Handbook of Chemistry and Physics*, 92nd ed.; CRC Press: Boca Raton, FL, 2011; p 2656.
(93) Nilsson, A.; Huang, C.; Pettersson, L. G. M. Fluctuations in ambient water. *J. Mol. Liq.* **2012**, *176*, 2−16.
(94) Finneran, I. A.; Carroll, P. B.; Allodi, M. A.; Blake, G. A. Hydrogen bonding in the ethanol-water dimer. *Phys. Chem. Chem. Phys.* **2015**, *17* (37), 24210−4.
(95) Ghanghas, R.; Jindal, A.; Vasudevan, S. Geometry of hydrogen bonds in liquid ethanol probed by proton NMR experiments. *J. Phys. Chem. B* **2020**, *124* (4), 662−667.
(96) Wang, Z.; Liu, K. H.; Harriger, L.; Leao, J. B.; Chen, S. H. Evidence of the existence of the high-density and low-density phases in deeply-cooled confined heavy water under high pressures. *J. Chem. Phys.* **2014**, *141* (1), 014501.
(97) Wang, Z.; Ito, K.; Leão, J. B.; Harriger, L.; Liu, Y.; Chen, S.-H. Liquid−liquid phase transition and its phase diagram in deeply-cooled heavy water confined in a nanoporous silica matrix. *J. Phys. Chem. Lett.* **2015**, *6* (11), 2009−2014.
(98) Hart, R. T.; Mei, Q.; Benmore, C. J.; Neuefeind, J. C.; Turner, J. F.; Dolgos, M.; Tomberli, B.; Egelstaff, P. A. Isotope quantum effects in water around the freezing point. *J. Chem. Phys.* **2006**, *124* (13), 134505.
(99) Soper, A. K.; Benmore, C. J. Quantum differences between heavy and light water. *Phys. Rev. Lett.* **2008**, *101* (6), 065502.
(100) Millero, F. J.; Lepple, F. K. Isothermal compressibility of deuterium oxide at various temperatures. *J. Chem. Phys.* **1971**, *54* (3), 946−949.
(101) Badyal, Y. S.; Price, D. L.; Saboungi, M.-L.; Haeffner, D. R.; Shastri, S. D. Quantum effects on the structure of water at constant temperature and constant atomic density. *J. Chem. Phys.* **2002**, *116* (24), 10833−10837.
(102) Harris, K. R.; Woolf, L. A. Temperature and volume dependence of the viscosity of water and heavy water at low temperatures. *J. Chem. Eng. Data* **2004**, *49* (4), 1064−1069.
(103) Harris, K. R.; Woolf, L. A. Temperature and volume dependence of the viscosity of water and heavy water at low temperatures (vol 49, pg 1064, 2004). *J. Chem. Eng. Data* **2004**, *49* (4), 1851−1851.
(104) Kim, K. H.; Pathak, H.; Späh, A. Temperature-independent nuclear quantum effects on the structure of water. *Phys. Rev. Lett.* **2017**, *119* (7), 075502 DOI: 10.1103/PhysRevLett.119.075502.
(105) Fumagalli, L.; Esfandiar, A.; Fabregas, R.; et al. Anomalously low dielectric constant of confined water. *Science* **2018**, *360* (6395), 1339−1342.
(106) Senapati, S.; Chandra, A. Molecular dynamics simulations of simple dipolar liquids in spherical cavity: Effects of confinement on structural, dielectric, and dynamical properties. *J. Chem. Phys.* **1999**, *111* (3), 1223−1230.
(107) Senapati, S.; Chandra, A. Dielectric constant of water confined in a nanocavity. *J. Phys. Chem. B* **2001**, *105* (22), 5106−5109.
(108) Kim, Y.; Ding, H. R.; Zheng, Y. B. Investigating water/oil interfaces with opto-thermophoresis. *Nat. Commun.* **2022**, *13* (1), 3742.
(109) Svergun, D. I.; Richard, S.; Koch, M. H. J.; Sayers, Z.; Kuprin, S.; Zaccai, G. Protein hydration in solution: Experimental observation by X-ray and neutron scattering. *Proc. Natl. Acad. Sci. U. S. A.* **1998**, *95* (5), 2267−2272.
(110) Gonella, G.; Backus, E. H. G.; Nagata, Y.; et al. Water at charged interfaces. *Nat. Rev. Chem.* **2021**, *5* (7), 466−485.
(111) Pfeiffer, C.; Rehbock, C.; Hühn, D.; Carrillo-Carrion, C.; de Aberasturi, D. J.; Merk, V.; Barcikowski, S.; Parak, W. J. Interaction of colloidal nanoparticles with their local environment: The (ionic) nanoenvironment around nanoparticles is different from bulk and determines the physico-chemical properties of the nanoparticles. *J. R. Soc. Interface* **2014**, *11* (96), 20130931.
(112) Darlington, A. M.; Gibbs-Davis, J. M. Bimodal or trimodal? The influence of starting pH on site identity and distribution at the low salt aqueous/silica interface. *J. Phys. Chem. C* **2015**, *119* (29), 16560−16567.
(113) Zhu, S.; Qin, X.; Yao, Y.; Shao, M. pH-dependent hydrogen and water binding energies on platinum surfaces as directly probed through surface-enhanced infrared absorption spectroscopy. *J. Am. Chem. Soc.* **2020**, *142* (19), 8748−8754.
(114) Bruni, F.; Ricci, M. A.; Soper, A. K. Structural characterization of NaOH aqueous solution in the glass and liquid states. *J. Chem. Phys.* **2001**, *114* (18), 8056−8063.

(115) Botti, A.; Bruni, F.; Imberti, S.; Ricci, M. A.; Soper, A. K. Ions in water: The microscopic structure of concentrated NaOH solutions. *J. Chem. Phys.* **2004**, *120* (21), 10154−62.
(116) Mancinelli, R.; Botti, A.; Bruni, F.; Ricci, M. A.; Soper, A. K. Perturbation of water structure due to monovalent ions in solution. *Phys. Chem. Chem. Phys.* **2007**, *9* (23), 2959−67.
(117) Zhang, C. Y.; Yue, S. W.; Panagiotopoulos, A. Z.; Klein, M. L.; Wu, X. F. Dissolving salt is not equivalent to applying a pressure on water. *Nat. Commun.* **2022**, *13* (1), 822.
(118) Bogdan, N.; Vetrone, F.; Ozin, G. A.; Capobianco, J. A. Synthesis of ligand-free colloidally stable water dispersible brightly luminescent lanthanide-doped upconverting nanoparticles. *Nano Lett.* **2011**, *11* (2), 835−840.
(119) Barisik, M.; Atalay, S.; Beskok, A.; Qian, S. Size dependent surface charge properties of silica nanoparticles. *J. Phys. Chem. C* **2014**, *118* (4), 1836−1842.
(120) Abbas, Z.; Labbez, C.; Nordholm, S.; Ahlberg, E. Size-dependent surface charging of nanoparticles. *J. Phys. Chem. C* **2008**, *112* (15), 5715−5723.
(121) Wang, F.; Han, Y.; Lim, C. S.; et al. Simultaneous phase and size control of upconversion nanocrystals through lanthanide doping. *Nature* **2010**, *463* (7284), 1061−1065.

https://doi.org/10.1021/acs.jpclett.4c00044
J. Phys. Chem. Lett. 2024, 15, 2606−2615